PNAS RESEARCH ARTICLE | GENETICS OPEN ACCESS

Mutations in *MINAR2* encoding membrane integral NOTCH2-associated receptor 2 cause deafness in humans and mice

Guney Bademci[a], María Lachgar-Ruiz[b,c,d], Mangesh Deokar[e,f], Mohammad Faraz Zafeer[g], Clemer Abad[g], Muzeyyen Yildirim Baylan[h], Neil J. Ingham[b], Jing Chen[b], Claire J. Sineni[g], Nirmal Vadgama[i], Ioannis Karakikes[i], Shengru Guo[g], Duygu Duman[j], Nitu Singh[f], Gaurav Harlalka[e], Shirish P. Jain[e], Barry A. Chioza[k], Katherina Walz[a,g], Karen P. Steel[b], Jamal Nasir[l], and Mustafa Tekin[a,g,m,1]

Edited by Mary-Claire King, University of Washington, Seattle, WA; received March 8, 2022; accepted May 11, 2022

Discovery of deafness genes and elucidating their functions have substantially contributed to our understanding of hearing physiology and its pathologies. Here we report on DNA variants in *MINAR2*, encoding membrane integral NOTCH2-associated receptor 2, in four families underlying autosomal recessive nonsyndromic deafness. Neurologic evaluation of affected individuals at ages ranging from 4 to 80 y old does not show additional abnormalities. *MINAR2* is a recently annotated gene with limited functional understanding. We detected three *MINAR2* variants, c.144G > A (p.Trp48*), c.412_419delCGGTTTTG (p.Arg138Valfs*10), and c.393G > T, in 13 individuals with congenital- or prelingual-onset severe-to-profound sensorineural hearing loss (HL). The c.393G > T variant is shown to disrupt a splice donor site. We show that *Minar2* is expressed in the mouse inner ear, with the protein localizing mainly in the hair cells, spiral ganglia, the spiral limbus, and the stria vascularis. Mice with loss of function of the Minar2 protein (*Minar2*$^{tm1b/tm1b}$) present with rapidly progressive sensorineural HL associated with a reduction in outer hair cell stereocilia in the shortest row and degeneration of hair cells at a later age. We conclude that MINAR2 is essential for hearing in humans and mice and its disruption leads to sensorineural HL. Progressive HL observed in mice and in some affected individuals and as well as relative preservation of hair cells provides an opportunity to interfere with HL using genetic therapies.

autosomal recessive | deafness | hearing loss | MINAR2 | NOTCH2

Significance

Molecular components of hearing in mammalians are not completely delineated. Via a genetic approach conducted in families with sensorineural hearing loss, this study presents MINAR2 as an indispensable element of hearing in humans. Similarly, disruption of Minar2 in mice leads to progressive hearing loss associated with alterations in the stereocilia of hair cells, the receptors of hearing, while hair cells remain intact until later in life. We present *MINAR2* as a gene working in the inner ear that is essential for hearing in humans and mice. Degeneration of sensory epithelium is a common consequence of hereditary deafness precluding genetic therapies. The preservation of hair cells in mutant mice at young ages makes MINAR2 a good candidate for intervention.

Hearing loss (HL) is one of the most common sensory deficits, affecting ~1 in 500 newborns (1). Genetic factors are implicated in the majority of cases, with more than 80% of the inherited form exhibiting autosomal recessive transmission (2). No additional findings are present in over 70% of the cases, which are then classified as nonsyndromic HL (Hereditary Hearing Loss Homepage, https://hereditaryhearingloss.org/) (2, 3). Genetic testing for etiologic evaluation has become a standard of care in people with congenital or childhood-onset sensorineural HL, which is caused by pathologies of the inner ear and auditory nerve (4, 5). Recent studies have shown that screening all recognized HL genes for variants reveals underlying cause in about half of the affected individuals, leaving a significant portion of people with HL with an unknown etiology (6–9). In the era of emerging genetic therapies for HL, finding the etiology of HL in affected individuals has become a critical task. This is especially relevant for progressive HL, as genetic therapies may potentially stop progression while cochlear hair cells are still alive (10–12).

MINAR2 (previously known as uncharacterized protein KIAA1024L and mouse gene *A730017C20Rik*) has recently been identified, and based on its structural similarity to MINAR1, named as major intrinsically disordered NOTCH2-associated receptor 2 or membrane integral NOTCH2-associated receptor 2 (13). A mutant mouse model of *Minar2* showed motor deficits similar to those seen in Parkinson disease, with no information about hearing abnormalities (13). A *Minar2* mutant mouse line, *Minar2*^{tm1b}, has also recently been reported to show no auditory brainstem responses at 14 wk old as part of a large HL screen (Mouse Genome Informatics [MGI]: 2442934) (11). Functional aspects of MINAR2 and consequences of its dysfunction in humans remain unknown.

In this study, to better map the landscape of hereditary HL, we sought DNA variants underlying deafness in 13 affected individuals from four families. We identified three different *MINAR2* variants in the families cosegregating with HL. We further showed that homozygous *Minar2*^{tm1b} mutant mice develop rapidly progressive HL associated with changes in outer hair cell stereocilia. Finally, via in vitro studies we demonstrated that *MINAR2* suppresses NOTCH2, suggesting that notch signaling might play a role in pathogenesis.

The authors declare no competing interest.

This article is a PNAS Direct Submission.

[1]To whom correspondence may be addressed. Email: mtekin@miami.edu.

This article contains supporting information online at http://www.pnas.org/lookup/suppl/doi:10.1073/pnas.2204084119/-/DCSupplemental.

Published June 21, 2022.

Results

Nonsyndromic Sensorineural HL Is Diagnosed in 13 Individuals from Four Unrelated Families. A summary of the auditory phenotype is shown in *SI Appendix*, Table S1. Ages ranged from 4 to 80 y old at the last examination. Each affected individual was diagnosed with HL either at birth or during infancy. Families 1 and 2 were of Turkish ancestry (Fig. 1). Parents of family 1 stated that in individuals II:1 and II:2, HL was milder in younger ages and progressed to a severe or profound degree by around age 10. Otoacoustic emissions were absent in these individuals. These siblings received unilateral cochlear implants at ages 12 and 10, respectively, which improved their oral communication. Individual II:3 in family 1 was diagnosed with profound sensorineural HL after failing the newborn hearing screening test. Otoacoustic emissions were absent at diagnosis. He received a unilateral cochlear implant at age 1 and communicates orally. Pure tone audiograms in parents showed normal thresholds (*SI Appendix*, Fig. S1).

Families 3 and 4 were of Indian ancestry. While there is no known consanguinity in any of the marriages in these two pedigrees, they are all from the same small town belonging to the same ethnic background, i.e., Hindu (religion) and Mali (Caste). All affected individuals in family 3 were born deaf and used signs, simple words, or sounds to be able to communicate. Severity of HL appeared to have remained the same in all the affected individuals from the beginning of life. Individuals IV:1 and IV:2 in family 4 were diagnosed with severe to profound sensorineural HL at the age of 3 y via auditory brainstem response (ABR) studies. Parents indicated a progression in the severity of HL. Their mode of communication at that age was predominantly nonverbal.

A high-resolution temporal bone CT scan or MRI was normal in at least one affected member of each family (*SI Appendix*, Fig. S1). None of the affected individuals had additional clinical findings for a syndromic form of deafness. Their neurodevelopmental skills were on target except for speech delay. None of the affected individuals showed impaired balance on tandem walking and Romberg test. Neurological examination was normal except for hearing loss in six affected individuals with ages ranging from 4 to 80 y. No affected individual was noted to have bradykinesia, tremor, or rigidity similar to those seen in Parkinson disease (*SI Appendix*, Table S2).

***MINAR2* Variants Cosegregate with Autosomal Recessive Deafness.** We performed genome sequencing in four affected individuals in families 1 (14) and 2 (15) and exome sequencing in three affected individuals in families 3 and 4 (Fig. 1*A*, individuals marked with an asterisk and *SI Appendix*, Table S3). Sequencing data in affected individuals were first analyzed for variants [single nucleotide variants (SNVs); insertions and/or deletions (indels); and copy number variants (CNVs) in recognized HL genes retrieved from the Hereditary Hearing Loss Homepage (https://hereditaryhearingloss.org/) (3), Online Mendelian Inheritance in Man (OMIM: https://omim.org/), University of Miami Molecular Genetics Laboratory HL gene panel, and a virtual gene panel for HL (v2.176) from PanelApp (https://www.genomicsengland.co.uk)]. Minor allele frequency (MAF) thresholds of 0.005 for recessive and 0.001 for dominant variants were used. Population allele frequencies were obtained from the genome aggregation database (gnomAD: https://gnomad.broadinstitute.org/) (16) and the single nucleotide polymorphism database (dbSNP: https://www.ncbi.nlm.nih.gov/projects/SNP/), as well as from our internal exome/genome database that includes >7,000 samples from different ethnicities. American College of Medical Genetics (ACMG) and ClinGen HL expert panel guidelines were followed for variant interpretation (17, 18). This analysis did not reveal a plausible variant under any inheritance model.

After excluding variants in previously recognized deafness genes, in family 1 we filtered shared homozygous coding and splice variants (SNVs, indels, and CNVs) in three affected siblings with a MAF of <0.005 in dbSNP, gnomAD highest subethnicity, and our internal control database. This filter reveals only a *MINAR2* (GeneBank: NM_001257308.2) c.412_419delCGGTTTTG (p.Arg138Valfs*10) variant in the family. The variant is located within a 9.4-MB shared homozygous run in three siblings, which is the only homozygous region >1 MB (*SI Appendix*, Tables S4 and S5). This frame-shift variant is predicted to introduce a premature stop codon and lead to early truncation of MINAR2.

In the proband of family 2, *MINAR2* is located within the second longest homozygous run at chromosome 5 (chr5):128,253,080 to 141,730,596 (hg19) (*SI Appendix*, Table S6). She is homozygous for the c.144G > A (p.Trp48*) variant in *MINAR2*. This nonsense variant is predicted to cause an early stop codon and result in truncation of MINAR2.

In the exome data of two affected individuals from family 3, filtering variants via the same criteria used in family 1 reveals only one variant for which both individuals are homozygous: *MINAR2* c.393G > T (p.Lys131Asn). SNP arrays show that this variant is located within the only shared homozygous run, >1 MB, in all seven affected individuals in family 3. This homozygous run is flanked by markers rs13174854 and rs377767449, which is 2.96 MB on chr5:128,738,407 to 131,705,915 (hg19). In family 4, two affected siblings share a 5.76-MB homozygous run on chr5: 126,978,108 to 132,742,450 (hg19), flanked by markers rs11241936 and rs11242152. Exome sequencing showed that the proband in family 4 is homozygous for the same *MINAR2* variant detected in family 3.

None of the detected *MINAR2* variants is listed in dbSNP or gnomAD databases and all variants are predicted to be deleterious (*SI Appendix*, Table S7). Sanger sequencing confirmed all three *MINAR2* variants and showed that each variant cosegregates with autosomal recessive HL in all families (Fig. 1*A*).

***MINAR2* c.393G > T (p.Lys131Asn) Leads to Aberrant Splicing.** While it is a missense change, the c.393G > T (p.Lys131Asn) variant substitutes the last nucleotide of exon 2, and is predicted to abolish a splice donor site (*SI Appendix*, Table S7 and Fig. S2). Via exon trapping experiments, we show that this variant leads to an addition of 85 intronic nucleotides into exon 2, which alters the amino acid composition of the rest of the protein leading to a premature stop codon (Fig. 1*D* and *SI Appendix*, Fig. S2). The same variant also leads to skipping of exon 2 entirely (Fig. 1*D*).

***Minar2*^{tm1b} Homozygous Mutant Mice Show Sensorineural HL.** To prove causality of disruption of Minar2 in sensorineural HL, we evaluated hearing in *Minar2* mutant mice. Hearing sensitivity of *Minar2*^{tm1b} mutant mice (*SI Appendix*, Fig. S3) was assessed using two methods: ABR, a measure of neural activity in the auditory nerve and brainstem, and distortion product otoacoustic emission (DPOAE), a measure of outer hair cell electromotility and resulting nonlinearities in the cochlea. Thresholds for both ABRs and DPOAEs were raised in homozygous mutants compared with wild-type littermates from the earliest age studied, postnatal day (P) 14, only 2 d after the usual onset of hearing (Fig. 2). By 4 wk old, the

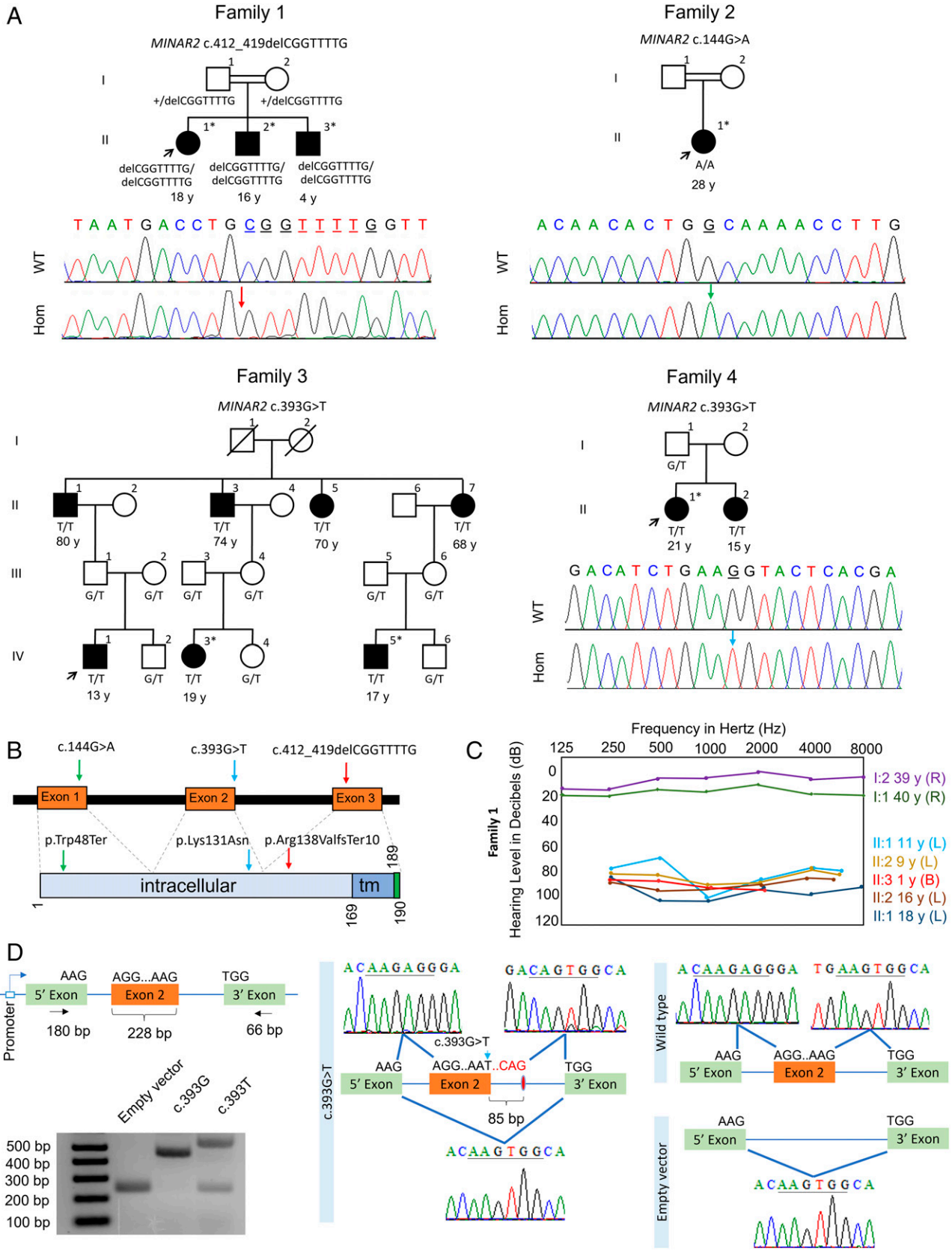

Fig. 1. Families, *MINAR2* variants, and the effects of the c.393G > T variant on splicing. (*A*) Pedigrees and segregation of the *MINAR2* variants in families. Filled symbols denote affected individuals and double lines indicate first cousin consanguinity. Electropherograms show the identified variant. The wild-type traces are from an unrelated individual. WT, wild type; Hom, homozygous mutant; exome/genome sequencing was performed in individuals marked with an (*) asterisk. (*B*) Locations of the identified variants. Tm, transmembrane. (*C*) Audiogram of family 1 (R, right ear; L, left ear; B, bilateral). (*D*) *MINAR2* exon 2 inserted into a vector consisting of 5′ and 3′ exons in the exon trap assay is shown. There are larger and smaller PCR products in the c.393G > T sample compared to wild type. Sanger sequencing confirms insertion of 85 bp at the donor site of exon 2 and skipping of exon 2.

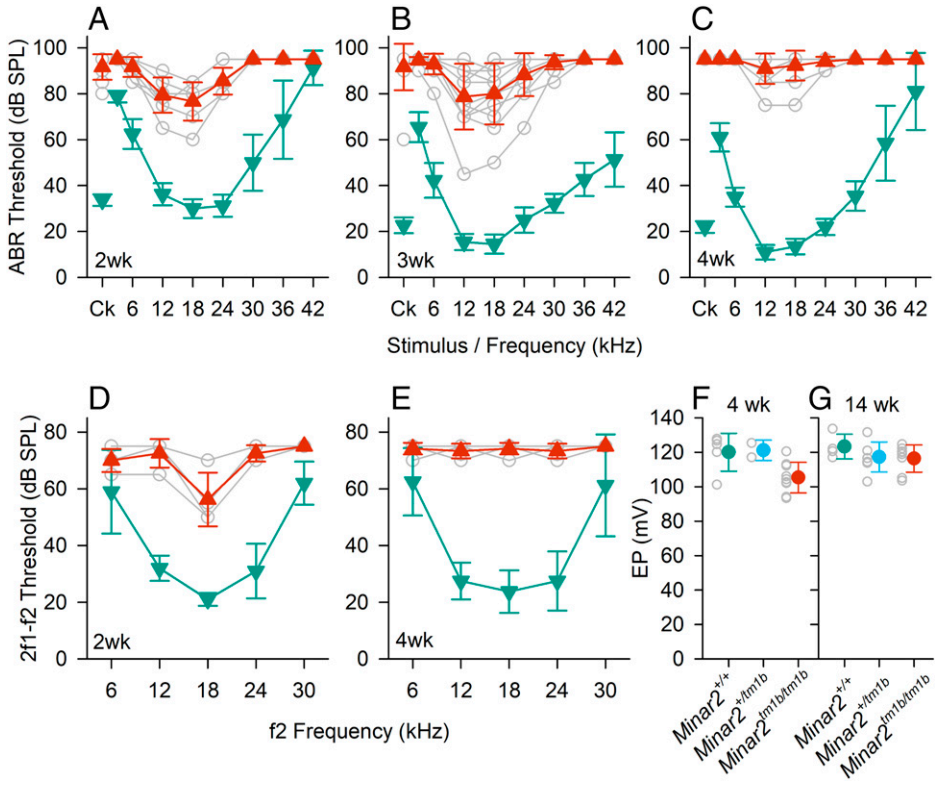

Fig. 2. Auditory studies in *Minar2* mutant mice. (*A*–*C*) ABR thresholds. Mean (±SD) ABR thresholds are plotted against stimulus for $Minar2^{+/+}$ mice (teal, down triangles) and $Minar2^{tm1b/tm1b}$ mice (red, up triangles). Open gray circles indicate thresholds for individual $Minar2^{tm1b/tm1b}$ mice. Results are plotted for data obtained at P14 (*A*) (n = 4 $Minar2^{+/+}$, 9 $Minar2^{tm1b/tm1b}$); P21. (*B*) (n = 11 $Minar2^{+/+}$, 12 $Minar2^{tm1b/tm1b}$ and P27 to P28 (*C*) (n = 10 $Minar2^{+/+}$, 11 $Minar2^{tm1b/tm1b}$). Ck, click. (*D* and *E*) DPOAE thresholds. Mean (±SD) DPOAE thresholds are plotted against f2 stimulus frequency for *Minar2* control mice (teal, down triangles) and $Minar2^{tm1b/tm1b}$ mice (red, up triangles). Open gray circles indicate thresholds for individual $Minar2^{tm1b/tm1b}$ mice. Results are plotted for data obtained at P14 (*D*) (n = 4 controls, comprising 1 wild type and 3 heterozygotes, n = 4 mutants) and P27 to P28 (*E*) (n = 4 wild types, n = 6 mutants). (*F* and *G*) EP in *Minar2* mutant mice aged 4 wk (*F*) and 14 wk old (*G*). Colored circles indicate the mean (±SD) EP measurement in $Minar2^{+/+}$ (teal), $Minar2^{+/tm1b}$ (cyan), and $Minar2^{tm1b/tm1b}$ (red) mice. Open gray circles indicate the EP values recorded in individual mice. At 4 wk old (P30 to P32) $Minar2^{+/+}$ n = 5, range 101.2 to 127.8 mV; $Minar2^{+/tm1b}$ n = 2 range 117.0 to 125.4 mV; and $Minar2^{tm1b/tm1b}$ n = 9, range 93.4 to 120.5 mV. At 14 wk old $Minar2^{+/+}$ n = 4, range 117 to 133.6 mV; $Minar2^{+/tm1b}$ n = 7, range 113.8 to 131.6 mV; and $Minar2^{tm1b/tm1b}$ n = 8, range 103.5 to 124.7 mV.

mutant mice showed severe elevations in threshold or no response at the highest sound levels used. Endocochlear potential was only slightly reduced from a mean of 120 mV to 105 mV in $Minar2^{tm1b/tm1b}$ mice, with most mutant mice exhibiting an endocochlear potential (EP) in the normal physiological range for mice of over 100 mV (Fig. 2).

***Minar2* Is Expressed in the Mouse Cochlea.** To further understand the role of Minar2 in hearing, we assessed the presence of *Minar2* transcript in different mouse tissues, including the inner ear, and specifically the cochlea. Total RNA was isolated from wild-type mice at embryonic day (E) 18.5, P0, and P30. RT-PCR with a forward primer located in exon 2 and a reverse primer in exon 3 of the *Minar2* gene (GenBank: NM_173759) produced a unique band of 171 bp corresponding to the wild-type mRNA in all analyzed tissues, with the exception of the liver. We find that *Minar2* is highly expressed in the inner ear, and specifically in the cochlea, at E18.5, P0, and P30 (Fig. 3*A*). To determine specific locations of *Minar2* expression within the cochlea, we proceeded to study $Minar2^{tm1b}$ heterozygous mutant mice taking advantage of the reporter gene. β-Galactosidase staining of P1 cross-sections and whole mount organ of Corti preparations reveals that *Minar2* is mainly localized in the hair cells, the supporting cells, spiral ganglion (including the nerve fibers), the spiral limbus, and the stria vascularis (Fig. 3*B* and *SI Appendix*, Fig. S4 *A* and *B*). Of note, the gene expression analysis resource (gEAR; https://umgear.org/) portal shows *Minar2* expression both in hair cells and supporting cells (*SI Appendix*, Fig. S4*C*) (19, 20). Double labeling for Minar2 and Tuj1 in heterozygous mutant mice shows that the two are expressed in different cell types and Minar2 is not present in the neurons of the spiral ganglion that were marked with Tuj1, suggesting that Minar2 is located in spiral ganglion glial cells (Fig. 3 *C*, *E*, and *F*).

The Earliest Defect in $Minar2^{tm1b}$ Mutant Mice Appears in Stereocilia Bundles. We used scanning electron microscopy (SEM) (Fig. 4) to examine the cochlea of mice aged 14 d old because at this age the ABR thresholds were raised but synapses appeared normal in numbers (Fig. 5). The organization of the organ of Corti appeared normal and there were very few missing stereocilia bundles in mutants, suggesting that hair cell degeneration cannot explain the raised ABR thresholds at this age (*SI Appendix*, Fig. S5). However, when we examined the stereocilia bundles of outer hair cells, we saw the shortest row was depleted, with reduced numbers and abnormally short stereocilia (Fig. 4). Outer hair cells along the entire length of the cochlear duct showed this feature. Inner hair cells appeared close to normal, although the middle row of stereocilia occasionally appeared more irregular than in the control littermates. Heterozygotes looked the same as wild-type littermates at this age.

Mechanoelectrical Transduction Channels Are Functional in $Minar2^{tm1b/tm1b}$ Mice. To study the mechanoelectrical transduction (MET), we used the FM1-43 FX dye, a molecule commonly used to assay the MET channel function, since functional MET

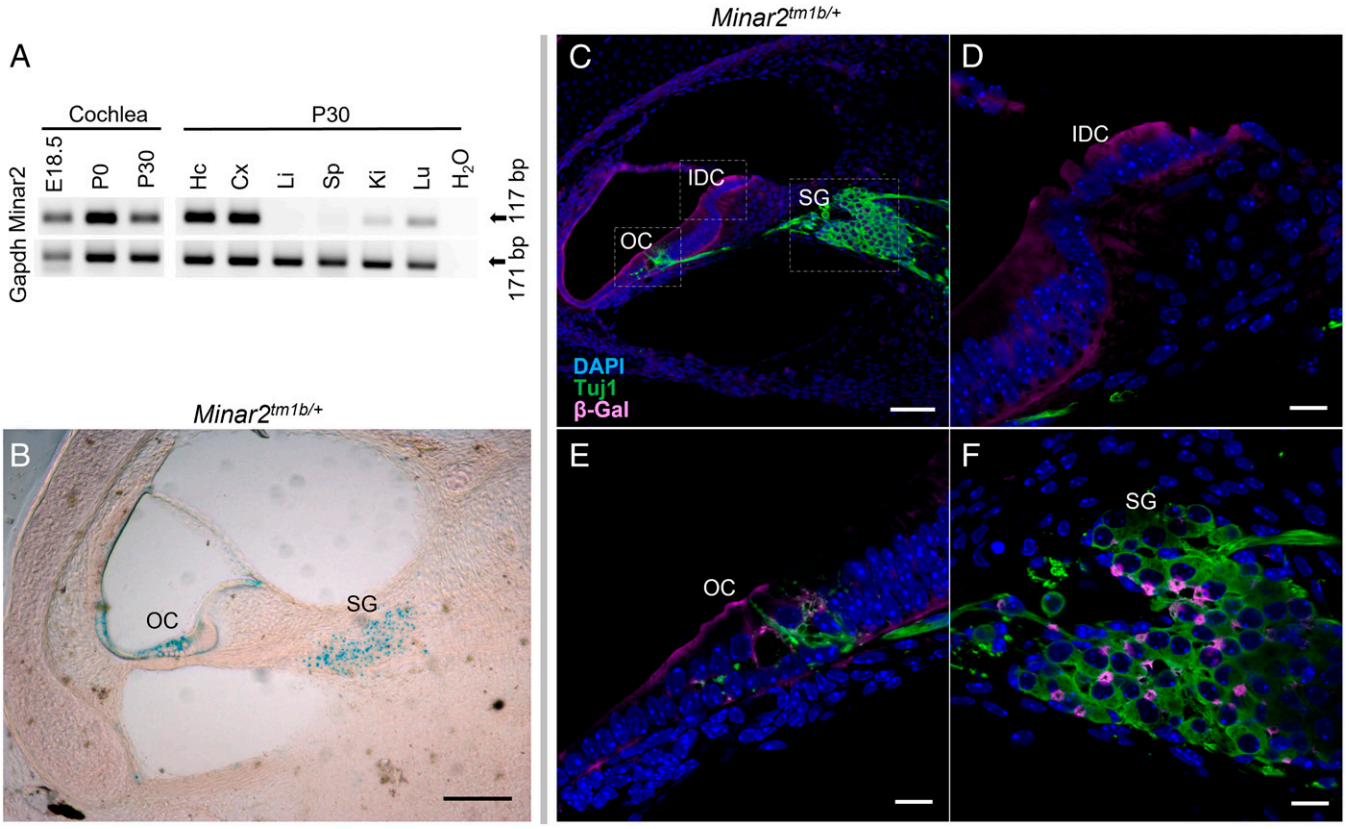

Fig. 3. Expression of *Minar2*, localization of the protein in the cochlea and innervation of cochlear hair cells in *Minar2* heterozygous mice, using the *LacZ* reporter gene component of the inserted cassette in the mutant allele, which expresses β-galactosidase (*SI Appendix*, Fig. S3). (*A*) RT-PCR of *Minar2* expression in the cochlea at E18.5, P0, and P30. Also, expression in different mouse tissues at P30 are Hc, hippocampus; Cx, cortex; Li, liver; Sp, spleen; Ki, kidney; Lu, lung. Gapdh was used as a control. (*B*) Localization of *Minar2* using the reporter gene LacZ of the mutant allele and in β-gal staining shown in blue. Note the localization of Minar2 at the SG, spiral ganglion; OC, organ of Corti. (Scale bar: 70 μm.) (*C*) Cross-section from 24-kHz region of P1 mutant inner ear was labeled with anti–β-gal (magenta) to detect Minar2 localization and Tuj1 (green) to label neurons. (Scale bar: 70 μm in *C*.) A zoom in is shown in *D*–*F*. (Scale bars: 10 μm.) IDC, interdental cells.

channels are required for the uptake of this fluorescent dye into the hair cells (21). We perfused cochleae from P14 mice and observed FM1-43 FX dye uptake by both inner and outer hair cells in $Minar2^{+/+}$ and $Minar2^{tm1b/tm1b}$ mice. Heterozygotes looked the same as wild-type littermates. While the intensity of the staining varied from mouse to mouse, all the samples showed

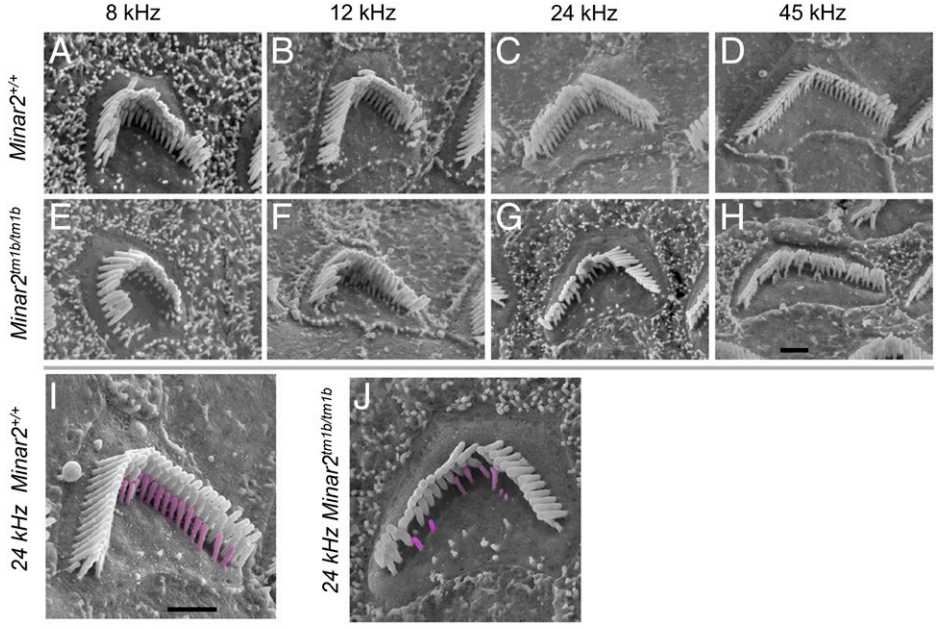

Fig. 4. Scanning electron microscopy reveals stereocilia defects. Outer hair cells at 8 kHz (85% of distance from base), 12 kHz (70%), 24 kHz (40%), and 45 kHz (20%) best frequency locations in wild-type mice (*A*–*D*) and $Minar2^{tm1b}$ homozygotes (*E*–*H*). Higher magnification images with the shortest row colored in magenta in a wild-type (*I*) and a mutant (*J*) outer hair cell, showing the reduction in numbers. (Scale bars in *H* and *I*: 1 μm.)

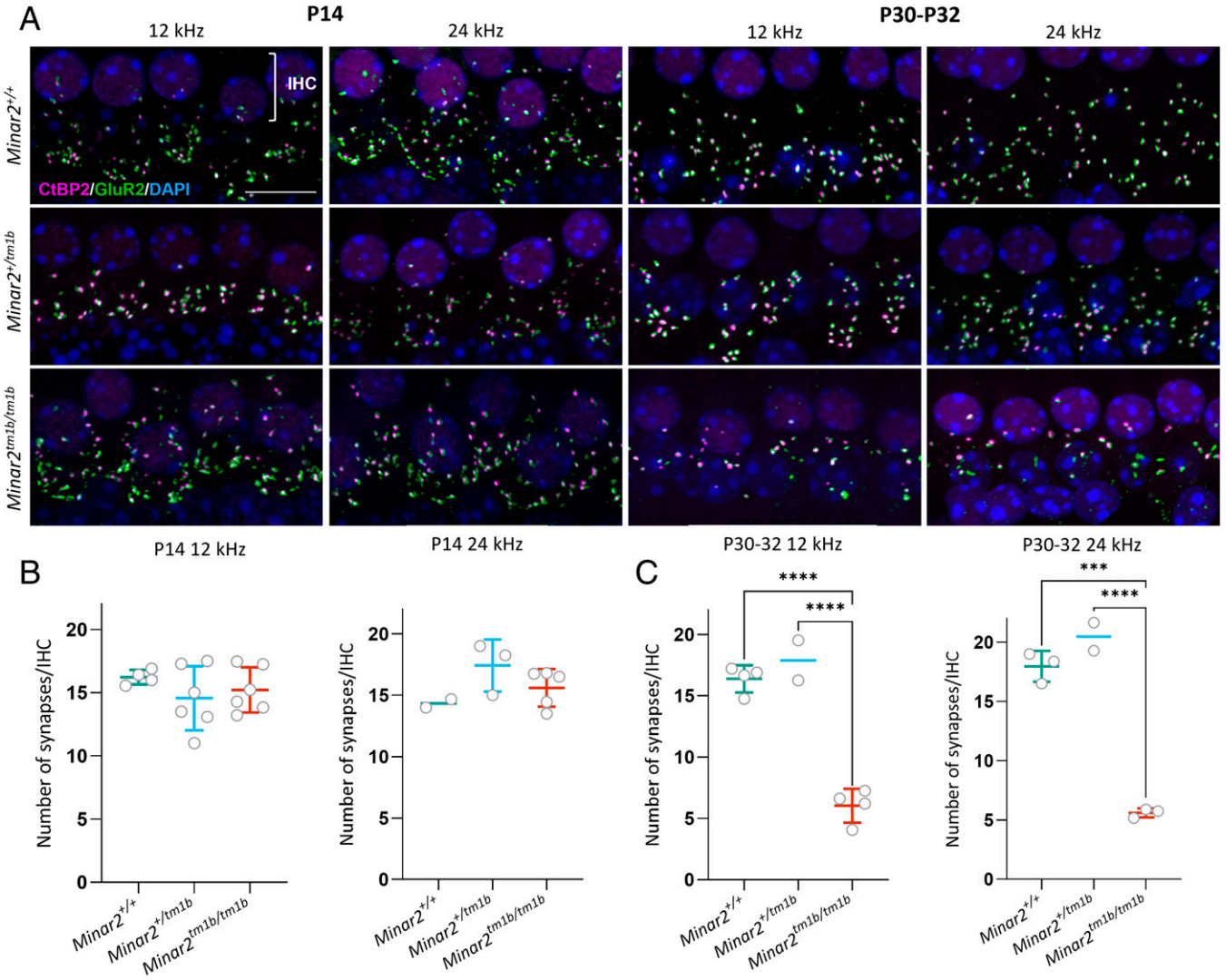

Fig. 5. Synaptic abnormalities of cochlear hair cells in *Minar2* mutant mice. (*A*) Synapses were examined using anti-CtBP2 antibody to mark presynaptic ribbons (magenta) and anti-GluR2 antibody to mark postsynaptic densities (green). Nuclei are shown in blue (DAPI). (Scale bar: 5 μm.) The images correspond to the cochlear best-frequency regions of 12 kHz and 24 kHz. The row of nuclei at the *Top* of each image corresponds to the IHCs. (*B* and *C*) Quantification of ribbon synapses per IHC at P14 (*B*) and P30 to P32 (*C*). Colocalized pre- and postsynaptic components were defined as a synapse. The average for each mouse is plotted as a circle. All data are shown as mean ± SD and statistically analyzed by one-way ANOVA with multiple comparisons. At P14, no significant difference was seen between homozygotes ($n = 6$ at 12 kHz and $n = 5$ at 24 kHz) and heterozygotes ($n = 6$ at 12 kHz and $n = 3$ at 24 kHz) or wild types ($n = 4$ at 12 kHz and $n = 2$ at 24 kHz). At P30 to P32, there are significantly fewer colocalized synapses in *Minar2*$^{tm1b/tm1b}$ ($n = 4$ for 12 kHz and $n = 3$ for 24 kHz) compared to wild types ($n = 4$ at 12 kHz and $n = 3$ at 24 kHz) and compared to heterozygotes ($n = 2$). ***$P = 0.0001$ and ****$P < 0.0001$.

uptake of the molecule specifically in hair cells, indicating that the MET channels are active in the *Minar2* mutants (*SI Appendix*, Fig. S6).

Hair Cell Degeneration Is a Secondary Feature in *Minar2*^{tm1b} Mutant Mice. Hair cell degeneration is a common feature in HL, and extensive loss of hair cells may preclude some approaches to treatments. Therefore, we examined older *Minar2*^{tm1b} mutant mice, aged 14 wk, to assess the loss of hair cells. We have previously reported that these mutants show no auditory brainstem responses at 14 wk old (11) and the EP is normal at this age (Fig. 2*G*). At earlier ages we see minimal evidence of any hair cell degeneration (*SI Appendix*, Fig. S5). However, by 14 wk of age, there is extensive loss of hair cells, with some discrete patches distributed along the length of the cochlear duct where the entire organ of Corti appears to have degenerated while other regions show scattered missing hair cells, both inner and outer, within the organ of Corti (Fig. 6). Heterozygotes had a similar appearance to the wild-type mice.

***Minar2*^{tm1b} Mutant Mice Show Reduction in the Number of Inner Hair Cell Ribbon Synapses at P30.** To understand underlying pathophysiology further, we evaluated the innervation pattern of hair cells by staining neurons with an anti-neurofilament antibody in the organ of Corti at P1 (*SI Appendix*, Fig. S7). Homozygous mutant mice show an altered innervation pattern of hair cells with a reduction in the nerve fibers around inner hair cells and a dispersed distribution of nerve fibers toward outer hair cells. *Minar2*^{tm1b} mutant mice show reduction in the number of crossings of type II nerves at P14 (Fig. 7). We subsequently examined synapses of inner hair cells using anti-CtBP2 antibody to label presynaptic ribbons and anti-GluR2 antibody to mark the AMPA receptor subunit R2, a part of the postsynaptic density. Ribbon synapses look qualitatively normal at both ages tested, P14 and P30, and the number of synapses per inner hair cell in homozygous mutants was not significantly different from numbers in heterozygotes or wild-type controls at P14, indicating that the raised ABR thresholds observed at that age in mutants are not due to the

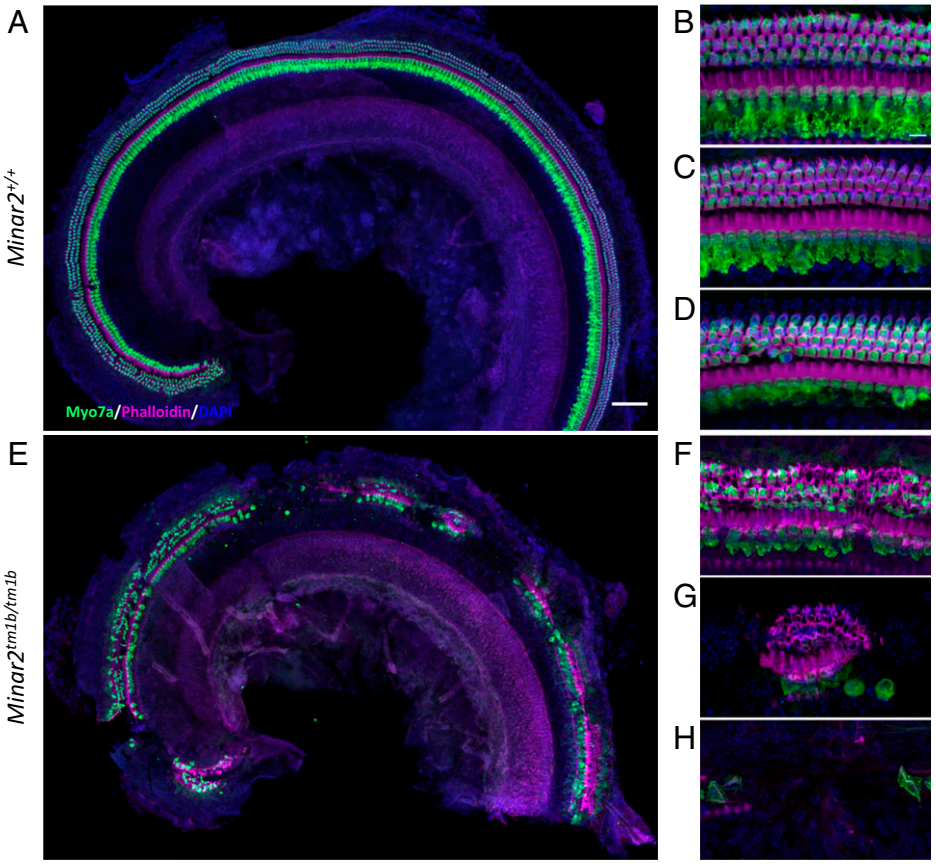

Fig. 6. Hair cell degeneration pattern in *Minar2*^{tm1b} mutant mice at 14 wk old. Confocal maximum intensity projection images of the whole-mount organ of Corti of 14-wk-old mice. Hair cells were examined using anti-Myo7a antibody (green) and phalloidin (magenta). Nuclei are shown in blue (DAPI). (Scale bars: 200 μm in *A* and 10 μm in *B*.) The images are representative examples of *Minar2*$^{+/+}$ (*A–D*) and *Minar2*$^{tm1b/tm1b}$ (*E–H*) mice. (*A* and *E*) Overview of the apical half of the cochlea. (*B–D*) High-magnification images corresponding to the 12 kHz, 24 kHz, and 36 kHz best-frequency regions, respectively. (*F–H*) High-magnification images of three different patterns of hair cell loss observed in *Minar2*^{tm1b} mutant mice. All five homozygotes that were studied at 14 wk old showed similar patches of loss of the organ of Corti at varying locations along the length of the cochlear duct interspersed with regions that showed only scattered hair cell loss. *Minar2*$^{+/+}$ ($n = 4$), *Minar2*$^{+/tm1b}$ ($n = 5$), and *Minar2*$^{tm1b/tm1b}$ ($n = 5$).

loss of ribbon synapses (Fig. 5 *A* and *B*). However, by P30 to P32 *Minar2*^{tm1b} mutant mice did show a significant decrease in the number of synapses compared to wild-type mice (Fig. 5 *A* and *C*), and this may contribute to the progression of HL.

Overexpression of *MINAR2* Suppresses Angiogenesis and MINAR2 Variants Abolish This Effect. As MINAR1 has been shown to inhibit angiogenesis (22), we investigated whether MINAR2 shows the same effect on angiogenesis in human umbilical vein endothelial cells (HUVEC). These studies reveal that transient overexpression of *MINAR2* suppresses angiogenesis (Fig. 8*A*). In addition, overexpressing each *MINAR2* variant detected in families 1 and 2 in HUVEC reduces suppression of angiogenesis, suggesting that they are loss-of-function variants (Fig. 8*A*).

Expression Levels of *MINAR2* Are Inversely Correlated with Intracellular NOTCH2 Abundance. MINAR2 is named based on its structural similarity to MINAR1, which is shown to be involved in NOTCH2 signaling (22). While MINAR2 is a much smaller protein compared to MINAR1 (190 vs. 917 amino acids) (22), it has recently been shown to bind NOTCH2 in a coimmunoprecipitation assay (13). Thus, we set out to explore whether NOTCH2 abundance in cells is correlated with *MINAR2* expression (23, 24). Furthermore, as NOTCH and VEGF signaling pathways are known to interact during angiogenesis (25), we determined the effect of *MINAR2* expression on VEGF. Our studies show that overexpression of wild-type *MINAR2* in HUVEC is associated with reduced abundance of NOTCH2 and VEGFA (a prominent VEGF protein in vascular endothelial cells) (Fig. 8*B*). Silencing of *MINAR2* in PC12 cells, which endogenously express *MINAR2*, leads to an increase in NOTCH2 and confirms the suppressor effect of *MINAR2* on NOTCH2 abundance (Fig. 8*C* and *SI Appendix*, Fig. S8).

MINAR2 Is Involved in MAP Kinase and mTOR Pathways. MINAR1 has been shown to regulate neurite outgrowth in a neuroendocrine cell line PC12 (26), in which neurite outgrowth via nerve growth factor is achieved by MAPK and PI3K pathways (27). The mTOR complex is a downstream target of PI3K, which contains mTORC1 and mTORC2 complexes in its central catalytic domain (26). We tested the effects of MINAR2 on the MAPK pathway by transiently overexpressing wild-type *MINAR2* in PC12 cells and detecting levels of ERK1/2 and pERK1/2, a crucial kinase of the MAPK signaling pathway. These studies show that overexpression of wild-type *MINAR2* reduces the abundance of pERK1/2, the active form of ERK1/2. On the other hand, overexpression of the two *MINAR2* deafness variants in families 1 and 2 does not show this effect, again supporting their loss of function (*SI Appendix*, Fig. S9*A*). When we silenced *MINAR2* in PC12 cells, we observed an increase in a functional protein in mTORC1 activity, P-S6, at 12 h (*SI Appendix*, Fig. S9*B*). However, there was

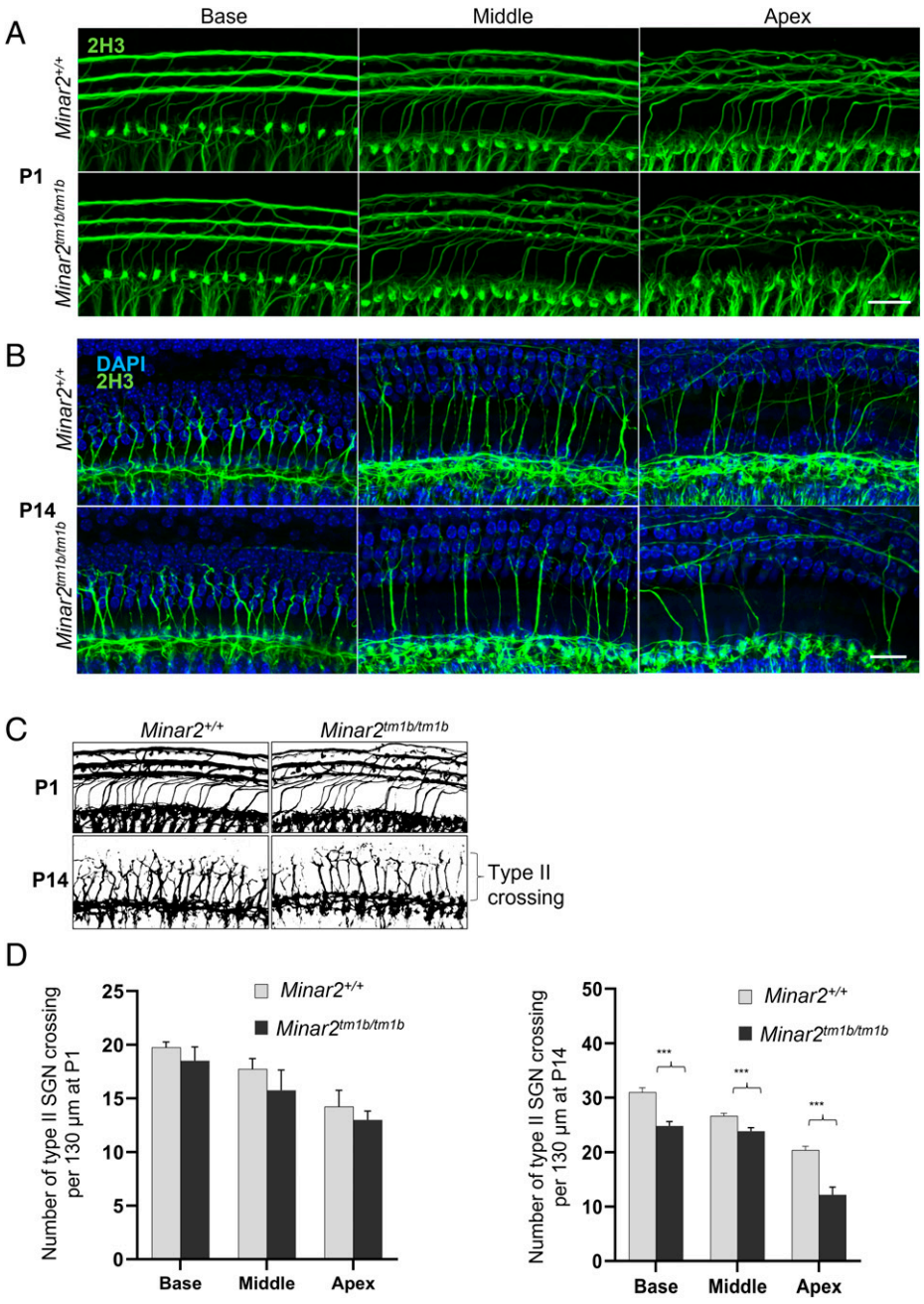

Fig. 7. Confocal maximum intensity projection images from a 24-kHz region of the whole-mount cochlea. (*A* and *B*) Total innervation with anti-2H3 neurofilament label (green) for P1 and P14 ($n = 3$ each group) wild-type and mutant mice. (Scale bars in *A* and *B*: 20 µm.) (*C*) Schematic diagram of whole-mount cochlea, demonstrating the innervation pattern of type II nerves at P1 and P14 wild-type and mutant mice. (*D*) The total number of crossings of type II nerves is show as histogram ($n = 3$; ***$P < 0.001$.)

no difference in pAKT, a component of mTORC2 activity (*SI Appendix*, Fig. S9*B*).

Discussion

In this study we present three loss-of-function variants in *MINAR2* in four families cosegregating with nonsyndromic sensorineural HL. Hearing loss started at birth or in early childhood in all 13 affected individuals. A progressive HL reaching a severe-to-profound degree during childhood was noted in four affected individuals. In addition to ABR thresholds showing sensorineural HL, otoacoustic emissions were absent in three children tested, suggesting dysfunction of both inner hair cell/acoustic nerve and outer hair cells. To support causality of the *MINAR2* mutations in deafness and to begin understanding the mechanism of HL, we show that *Minar2*$^{tm1b/tm1b}$ mice have a severe, progressive increase in ABR thresholds from 2 wk old onwards (around the time that mice start to hear), with very few responses by 4 wk old. Otoacoustic emissions can be detected in the mutant mice but at raised thresholds at 2 wk old, and these responses are mostly absent by 4 wk old, implicating outer hair cells in the pathology. In conclusion, audiological findings both in humans and mice show that loss of MINAR2 function results in early-onset and sensorineural HL that rapidly progresses to severe to profound deafness.

The reduced number of stereocilia in the shortest row on outer hair cells would be expected to have a severe impact upon the number of transduction channel complexes available and suggests that the primary defect in these mutant mice is located at the top of the hair cell. However, we have demonstrated that

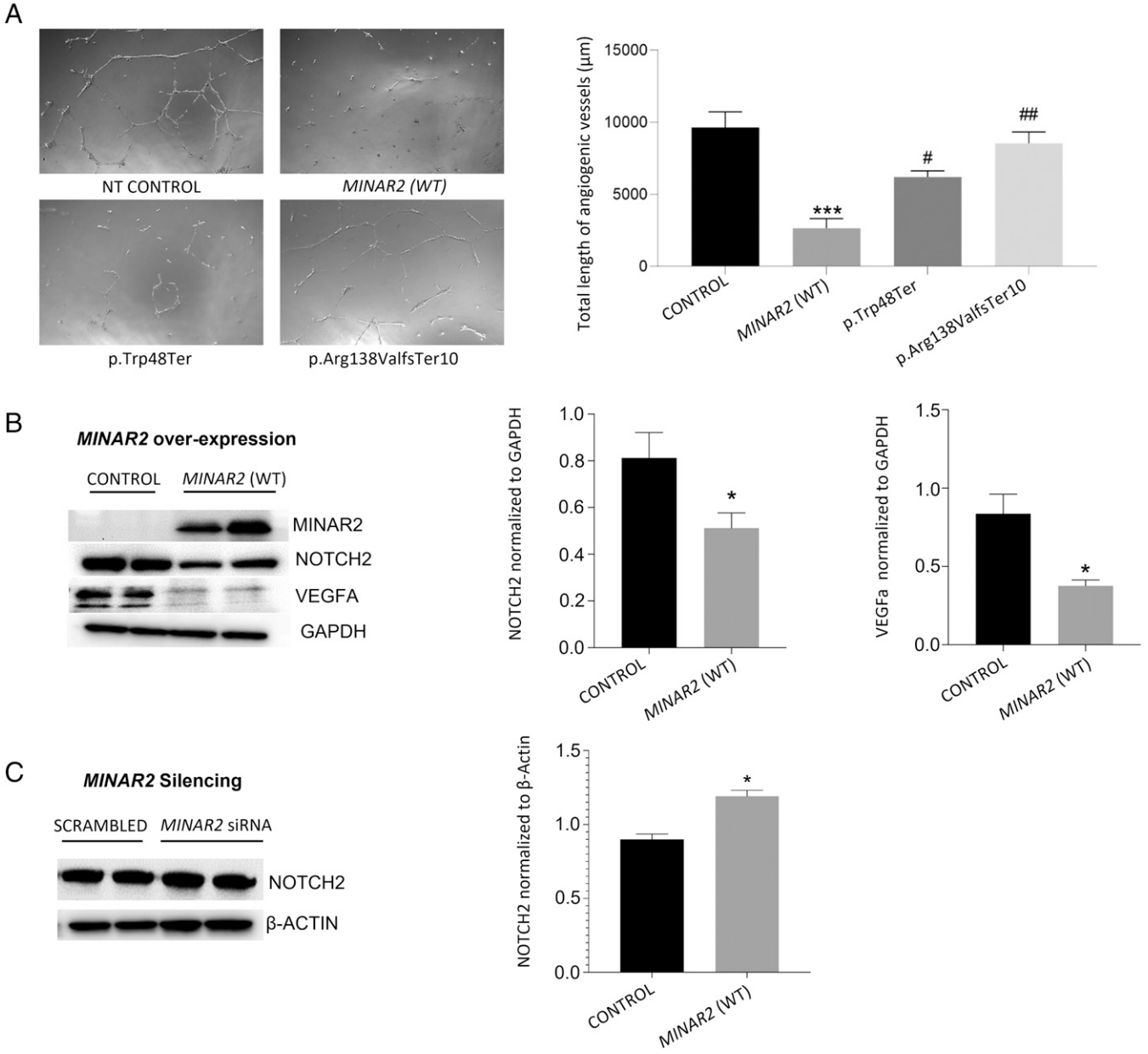

Fig. 8. Effects of *MINAR2* on angiogenesis, NOTCH2, and VEGFA. (*A*) Angiogenic potential of nontransfected (NT) HUVEC compared to cells transfected with *MINAR2* wild-type (WT), and *MINAR2* p.Trp48*, and p.Arg138Valfs*10 plasmid constructs. *Right* graph shows analysis of total length of angiogenic vessels formed after incubation of 12 h on Matrigel-coated wells; images were analyzed with ImageJ angioanalyzer and results are expressed as mean ± SEM. Significant differences were shown as $^{***}P \leq 0.001$ when compared to control and as $^{\#\#}P \leq 0.01$ when compared to *MINAR2(WT)*. (*B*, *Left*) Immunoblot images showing the effect of *MINAR2(WT)* transient overexpression on NOTCH2 and VEGFA protein levels in HUVEC cells. (*Right*) Statistical analysis of GAPDH-normalized relative protein expressions of NOTCH2 and VEGFA. Results are expressed as mean ± SEM and significant differences are shown as $^{*}P \leq 0.05$ when compared to control. (*C*, *Left*) Immunoblot images of siRNA-induced MINAR2 silencing on NOTCH2 protein levels in PC12 cells. (*Right*) β-Actin normalized relative protein expression of NOTCH2. Results are expressed as mean ± SEM and significant differences are shown as $^{*}P \leq 0.05$ when compared to control. Data were analyzed by one-way ANOVA with multiple comparisons.

the remaining MET channels are active in *Minar2*$^{tm1b/tm1b}$ mice, since the hair cells of these mice are able to uptake FM1-43 dye. Degeneration of hair cells (Fig. 6) and synaptic defects (Fig. 5) occur later in development and cannot explain the raised ABR and DPOAE thresholds at 14 d old in the *Minar2*^{tm1b} homozygotes. Mutations of other genes also lead to loss of the shorter stereocilia associated with hearing impairment, for example the *Baiap2l2* mutant (28) and the *Clrn2* mouse mutant (29).

The Notch pathway is a highly conserved intercellular signaling cascade that is activated by the interaction of transmembrane ligands (Delta and Jagged) with Notch receptors, which are usually expressed on the surface of neighboring cells. Binding of the Notch ligand to receptor induces cleavage of the Notch receptors intracellular domain, which binds to multiple DNA-binding proteins in the nucleus (30–32). In the initial stages of angiogenesis, Notch activation is generally repressed to allow proliferation of endothelial cells in response to VEGF stimulation, and its expression is later up-regulated when endothelial cells stop proliferating and the vessels begin to stabilize (33–39). While it is possible that the effects of MINAR2 on angiogenesis may play a role in hearing, we did not observe abnormal vascular structures in the cochlea of homozygous mutant mice. Moreover, the most sensitive part of the cochlea to vascular function is the generation of EP by the stria vascularis. In this study, EP was within the normal range in

homozygous mutant mice. Our results show that MINAR2 and NOTCH2 have a regulatory relationship. In the mammalian cochlea, there is no regeneration of sensory hair cells and the strictly controlled pattern of alternating hair cells and supporting cells in the organ of Corti is set up in early development. Notch signaling is believed to be a critical part of the process of cells deciding their fate as a hair cell or a supporting cell and many genes involved in Notch signaling underlie hearing impairment (40, 41). As our examination of the organ of Corti of young mice shows (*SI Appendix*, Fig. S5), the pattern is set up correctly, ruling out an early developmental defect of cell fate or differentiation. However, Notch signaling may also play a role in longer-term maintenance of the organ of Corti, and our findings of progressive deterioration of this organ resulting from mutation of a gene known to be involved in Notch signaling supports this suggestion.

MINAR family proteins (MINAR1 and MINAR2) have been proposed to be associated with the inhibition of cell proliferation (13, 22). In this study, we did not observe any proliferation effect in different ages of *Minar2*$^{tm1b/tm1b}$ mice. Terminal mitoses of hair cells occur early at E12 to E14 before birth (42). The confocal images illustrated in Fig. 6 all indicate loss of cells from the normal regular array, with no sign of any proliferation.

Our findings of an abnormal innervation pattern of hair cells as early as P1, as well as a significant decrease in the numbers of intact synapses at 4 wk old, suggest that abnormal innervation of hair cells may contribute to the severe auditory dysfunction in *Minar2*$^{tm1b/tm1b}$ mice. Based on these findings, Minar2 may be playing a role in the maintenance of hair cell synapses. MINAR2 is structurally similar to MINAR1, which has been reported to be involved in controlling neurite formation during neuronal differentiation through DEP domain containing MTOR interacting protein (DEPTOR). In this study, we show that similar to MINAR1, MINAR2 down-regulates mTOR signaling (*SI Appendix*, Fig. S9*B*), which may contribute to the abnormal innervation pattern observed in the organ of Corti of *Minar2* mutant mice.

It is notable that although the sensory hair cells are present up to 4 wk old and are able to take up FM1-43 dye through transduction channels, they do not appear to be functioning normally as shown by the raised ABR and DPOAE thresholds. Most genetic and environmental causes of sensorineural HL lead to permanent loss of hair cells, reducing the chance of gene therapy or gene editing approaches. Progressive HL associated with a relatively normal appearance of hair cells in young ages makes *MINAR2* a promising target for genetic therapies. Further elucidation of its role in the maintenance of hair cell synapses and stereocilia bundles may open new avenues to treat more common forms of HL resulting from similar mechanisms.

Materials and Methods

More details of materials and methods are in *SI Appendix*.

Study Approval. This study was approved by the University of Miami Institutional Review Board (20081138-USA), as well as by the Ethics Committees of Ankara University Medical School (012413-Turkey) and Rajarshi Shahu College of Pharmacy (180720-India). A signed informed consent was obtained from all participants or, in the case of a minor, from the parents.

DNA Sequencing and Bioinformatics Analysis. Genome sequencing was performed in family 1 individuals II:1, II:2, and II:3 and family 2 II:1 (Fig. 1*A* and *SI Appendix*, Table S3) (43, 44). Reads were mapped to human genome reference (National Center for Biotechnology Information [NCBI] build37/hg 19 version) with Burrows-Wheeler aligner (BWA). Genome Analysis Toolkit (GATK) was used for variant calling (45–47). CNVs were called using CNVnator (48). Enlis Genome Research software (https://www.enlis.com/) was used to identify runs of homozygosity in family 1 and family 2 from genome sequencing data (*SI Appendix*, Tables S4–S6).

Illumina Infinium Global Screening Array (GSA) v2 (Illumina) kit was used for genotyping in 16 members of family 3 and three members of family 4 to map the shared homozygous regions in affected individuals. Additional exome sequencing was performed on a HiSeq 2000 platform (Illumina), as described previously (49), in individuals IV:3 and IV:5 in family 3 and IV:1 in family 4 (*SI Appendix*, Table S3).

Genome sequencing data were deposited in the NCBI's BioProject database: PRJNA623118, BioSample: SAMN27763770 (family 1, individual II:1) and BioSample: SAMN27763769 (family 2, individual II:1).

Ethics Statement for Animals. Mouse studies in the United Kingdom were carried out in accordance with UK Home Office regulations and the UK Animals (Scientific Procedures) Act of 1986 (ASPA) under UK Home Office licenses, and the study was approved by the King's College London Ethical Review Committee. Mice were culled using methods approved under these licenses to minimize any possibility of suffering. All procedures in Miami were approved by the University of Miami Institutional Animal Care and Use Committee and followed the NIH guidelines "Using Animals in Intramural Research."

Mouse Generation. *Minar2*^{tm1a} mutant mice were generated at the Wellcome Sanger Institute by blastocyst microinjection of targeted embryonic stem (ES) cells on a C57BL/6N genetic background (50, 51). *Minar2*$^{tm1b(KOMP)Wtsi}$ mice (*Minar2*^{tm1b}) were generated from *Minar2*$^{tm1a(KOMP)Wtsi}$ mice by exposure of preimplantation embryos to soluble Cre recombinase (52), which leads to recombination between LoxP sites, removing the selection cassette and exon 2 to produce mice carrying the *Minar2*^{tm1b} allele (*SI Appendix*, Fig. S3). Both *tm1a* and *tm1b* alleles are available via the European Mouse Mutant Archive (EMMA; https://www.infrafrontier.eu).

Statistics. A one-way ANOVA with multiple comparisons was used to compare groups for count of synapses in mouse inner ear and also for angiogenesis, MAPK, and mTOR assays.

Data Availability. Sequencing data have been deposited in publicly accessible database, Family 1, II:1 (14) and Family 2, II:1 (15).

ACKNOWLEDGMENTS. We are immensely grateful to all the patients and families participating in this study. This study was supported by R01DC009645 and R01DC012836 from the NIH/National Institute on Deafness (M.T.), the National Institute for Health and Care Research Biomedical Research Centre, King's College London (K.P.S.), and the Royal National Institute for Deaf People (K.P.S.). This research was funded in part by the Wellcome Trust. For the purpose of Open Access, the author has applied a CC BY public copyright license to any Author Accepted Manuscript version arising from this submission. We thank the Wellcome Sanger Institute Mouse Genetics Project for generating and providing the *Minar2* mouse mutant. M.D. and G.H. would also like to express sincere gratitude for all the support provided by Dr. S. P. Jain, Principal, Rajarshi Shahu College of Pharmacy, Malvihir, Buldana, India.

Author affiliations: [a]Dr. John T. Macdonald Foundation Department of Human Genetics, University of Miami Miller School of Medicine, Miami, FL, 33136; [b]Wolfson Centre for Age-Related Diseases, King's College London, London, SE1 1UL, United Kingdom; [c]Servicio de Genética, Hospital Universitario Ramón y Cajal, IRYCIS, 28034 Madrid, Spain; [d]Centro de Investigación Biomédica en Red de Enfermedades Raras, 28034 Madrid, Spain; [e]Department of Pharmacology, Rajarshi Shahu College of Pharmacy, 443001 Malvihir, Buldana, India; [f]Oriental College of Pharmacy and Research, Oriental University, 453555 Indore, Madhya Pradesh, India; [g]John P. Hussmann Institute for Human Genomics, University of Miami Miller School of Medicine, Miami, FL 33136; [h]Department of Otorhinolaryngology, Faculty of Medicine, Dicle University, Diyarbakir 21200, Turkey; [i]Cardiovascular Institute and Department of Cardiothoracic Surgery, Stanford University School of Medicine, Stanford, CA, 94305; [j]Department of Audiology, Faculty of Health Sciences, Ankara University, Ankara 06100, Turkey; [k]College of Medicine and Health, University of Exeter Medical School, RD&E NHS Foundation Trust, Exeter, EX2 5DW, United Kingdom; [l]Molecular Biosciences Research Group, Faculty of Health and Society, University of Northampton, Northhampton, NN1 5PH, United Kingdom; and [m]Department of Otolaryngology, University of Miami Miller School of Medicine, Miami, FL, 33136

Author contributions: M.T. designed research; G.B., M.L.-R., M.D., M.F.Z., C.A., M.Y.B., N.J.I., J.C., C.J.S., N.V., I.K., S.G., D.D., N.S., G.H., S.P.J., B.A.C., K.W., K.P.S., J.N., and M.T. performed research; G.B., M.L.-R., N.J.I., K.P.S., and M.T. contributed new reagents/analytic tools; G.B., M.L.-R., M.D., M.F.Z., C.A., M.Y.B., N.J.I., J.C., C.J.S., N.V., I.K., S.G., D.D., N.S., G.H., S.P.J., B.A.C., K.W., K.P.S., J.N., and M.T. analyzed data; and G.B., M.L.-R., M.D., M.F.Z., C.A., N.J.I., N.V., G.H., K.W., K.P.S., J.N., and M.T. wrote the paper.

1. A. L. Mehl, V. Thomson, The Colorado newborn hearing screening project, 1992–1999: On the threshold of effective population-based universal newborn hearing screening. *Pediatrics* **109**, E7 (2002).
2. C. C. Morton, W. E. Nance, Newborn hearing screening–A silent revolution. *N. Engl. J. Med.* **354**, 2151–2164 (2006).
3. G. Van Camp, R. J. H. Smith, Hereditary Hearing Loss Homepage. https://hereditaryhearingloss.org. Accessed 1 December 2021.
4. R. L. Alford *et al.*; ACMG Working Group on Update of Genetics Evaluation Guidelines for the Etiologic Diagnosis of Congenital Hearing Loss; Professional Practice and Guidelines Committee, American College of Medical Genetics and Genomics guideline for the clinical evaluation and etiologic diagnosis of hearing loss. *Genet. Med.* **16**, 347–355 (2014).
5. A. M. Korver *et al.*, Congenital hearing loss. *Nat. Rev. Dis. Primers* **3**, 16094 (2017).
6. G. Bademci *et al.*, Comprehensive analysis via exome sequencing uncovers genetic etiology in autosomal recessive nonsyndromic deafness in a large multiethnic cohort. *Genet. Med.* **18**, 364–371 (2016).
7. J. Doll *et al.*, Genetic spectrum of syndromic and non-syndromic hearing loss in Pakistani families. *Genes (Basel)* **11**, 1329 (2020).
8. C. M. Sloan-Heggen *et al.*, Characterising the spectrum of autosomal recessive hereditary hearing loss in Iran. *J. Med. Genet.* **52**, 823–829 (2015).
9. D. Yan *et al.*, Spectrum of DNA variants for non-syndromic deafness in a large cohort from multiple continents. *Hum. Genet.* **135**, 953–961 (2016).
10. T. Atik, G. Bademci, O. Diaz-Horta, S. H. Blanton, M. Tekin, Whole-exome sequencing and its impact in hereditary hearing loss. *Genet. Res.* **97**, e4 (2015).
11. N. J. Ingham *et al.*, Mouse screen reveals multiple new genes underlying mouse and human hearing loss. *PLoS Biol.* **17**, e3000194 (2019).
12. B. Vona, I. Nanda, M. A. Hofrichter, W. Shehata-Dieler, T. Haaf, Non-syndromic hearing loss gene identification: A brief history and glimpse into the future. *Mol. Cell. Probes* **29**, 260–270 (2015).
13. R. X.-Y. Ho *et al.*, Loss of MINAR2 impairs motor function and causes Parkinson's disease-like symptoms in mice. *Brain Commun.* **2**, fcaa047 (2020).
14. M. Tekin, SRX15001233 Family 1, II:1. NCBI Sequence Read Archive. https://www.ncbi.nlm.nih.gov/sra/SRX15001233. Deposited 26 April 2022.
15. M. Tekin, SRX15001232: Family 2, II:1. NCBI Sequence Read Archive. https://www.ncbi.nlm.nih.gov/sra/SRX15001232. Deposited 26 April 2022.
16. K. J. Karczewski *et al.*; Genome Aggregation Database Consortium, The mutational constraint spectrum quantified from variation in 141,456 humans. *Nature* **581**, 434–443 (2020).
17. A. M. Oza *et al.*; ClinGen Hearing Loss Clinical Domain Working Group, Expert specification of the ACMG/AMP variant interpretation guidelines for genetic hearing loss. *Hum. Mutat.* **39**, 1593–1613 (2018).
18. S. Richards *et al.*; ACMG Laboratory Quality Assurance Committee, Standards and guidelines for the interpretation of sequence variants: A joint consensus recommendation of the American College of Medical Genetics and Genomics and the Association for Molecular Pathology. *Genet. Med.* **17**, 405–424 (2015).
19. R. Elkon *et al.*, RFX transcription factors are essential for hearing in mice. *Nat. Commun.* **6**, 8549 (2015).
20. J. Orvis *et al.*, gEAR: Gene Expression Analysis Resource portal for community-driven, multi-omic data exploration. *Nat. Methods* **18**, 843–844 (2021).
21. J. E. Gale, W. Marcotti, H. J. Kennedy, C. J. Kros, G. P. Richardson, FM1-43 dye behaves as a permeant blocker of the hair-cell mechanotransducer channel. *J. Neurosci.* **21**, 7013–7025 (2001).
22. R. X. Ho *et al.*, MINAR1 is a Notch2-binding protein that inhibits angiogenesis and breast cancer growth. *J. Mol. Cell Biol.* **10**, 195–204 (2018).
23. P. J. Lanford *et al.*, Notch signalling pathway mediates hair cell development in mammalian cochlea. *Nat. Genet.* **21**, 289–292 (1999).
24. W. Pan, Y. Jin, B. Stanger, A. E. Kiernan, Notch signaling is required for the generation of hair cells and supporting cells in the mammalian inner ear. *Proc. Natl. Acad. Sci. U.S.A.* **107**, 15798–15803 (2010).
25. A. F. Siekmann, L. Covassin, N. D. Lawson, Modulation of VEGF signalling output by the Notch pathway. *BioEssays* **30**, 303–313 (2008).
26. H. Zhang *et al.*, UBTOR/KIAA1024 regulates neurite outgrowth and neoplasia through mTOR signaling. *PLoS Genet.* **14**, e1007583 (2018).
27. D. Vaudry, P. J. Stork, P. Lazarovici, L. E. Eiden, Signaling pathways for PC12 cell differentiation: Making the right connections. *Science* **296**, 1648–1649 (2002).
28. A. J. Carlton *et al.*, Loss of Baiap2l2 destabilizes the transducing stereocilia of cochlear hair cells and leads to deafness. *J. Physiol.* **599**, 1173–1198 (2021).
29. L. A. Dunbar *et al.*, Clarin-2 is essential for hearing by maintaining stereocilia integrity and function. *EMBO Mol. Med.* **11**, e10288 (2019).
30. E. R. Andersson, R. Sandberg, U. Lendahl, Notch signaling: Simplicity in design, versatility in function. *Development* **138**, 3593–3612 (2011).
31. C. R. Chillakuri *et al.*, Structural analysis uncovers lipid-binding properties of Notch ligands. *Cell Rep.* **5**, 861–867 (2013).
32. F. M. Lu, S. E. Lux, Constitutively active human Notch1 binds to the transcription factor CBF1 and stimulates transcription through a promoter containing a CBF1-responsive element. *Proc. Natl. Acad. Sci. U.S.A.* **93**, 5663–5667 (1996).
33. A. M. Henderson, S. J. Wang, A. C. Taylor, M. Aitkenhead, C. C. Hughes, The basic helix-loop-helix transcription factor HESR1 regulates endothelial cell tube formation. *J. Biol. Chem.* **276**, 6169–6176 (2001).
34. F. Itoh *et al.*, Synergy and antagonism between Notch and BMP receptor signaling pathways in endothelial cells. *EMBO J.* **23**, 541–551 (2004).
35. K. G. Leong *et al.*, Activated Notch4 inhibits angiogenesis: Role of beta 1-integrin activation. *Mol. Cell. Biol.* **22**, 2830–2841 (2002).
36. Z. Liu *et al.*, Notch1 loss of heterozygosity causes vascular tumors and lethal hemorrhage in mice. *J. Clin. Invest.* **121**, 800–808 (2011).
37. M. Noseda *et al.*, Notch activation induces endothelial cell cycle arrest and participates in contact inhibition: Role of p21Cip1 repression. *Mol. Cell. Biol.* **24**, 8813–8822 (2004).
38. K. L. Taylor, A. M. Henderson, C. C. Hughes, Notch activation during endothelial cell network formation in vitro targets the basic HLH transcription factor HESR-1 and downregulates VEGFR-2/KDR expression. *Microvasc. Res.* **64**, 372–383 (2002).
39. S. E. Williams, S. Beronja, H. A. Pasolli, E. Fuchs, Asymmetric cell divisions promote Notch-dependent epidermal differentiation. *Nature* **470**, 353–358 (2011).
40. E. C. Driver, M. W. Kelley, Development of the cochlea. *Development* **147**, dev162263 (2020).
41. R. Brown, A. K. Groves, Hear, hear for notch: Control of cell fates in the inner ear by notch signaling. *Biomolecules* **10**, 370 (2020).
42. R. J. Ruben, Development of the inner ear of the mouse: A radioautographic study of terminal mitoses. *Acta Otolaryngol.* **220** (Suppl), 1–44 (1967).
43. G. Bademci *et al.*, FOXF2 is required for cochlear development in humans and mice. *Hum. Mol. Genet.* **28**, 1286–1297 (2019).
44. C. Li *et al.*, Dysfunction of *GRAP*, encoding the GRB2-related adaptor protein, is linked to sensorineural hearing loss. *Proc. Natl. Acad. Sci. U.S.A.* **116**, 1347–1352 (2019).
45. M. A. DePristo *et al.*, A framework for variation discovery and genotyping using next-generation DNA sequencing data. *Nat. Genet.* **43**, 491–498 (2011).
46. H. Li, R. Durbin, Fast and accurate long-read alignment with Burrows-Wheeler transform. *Bioinformatics* **26**, 589–595 (2010).
47. A. McKenna *et al.*, The Genome Analysis Toolkit: A MapReduce framework for analyzing next-generation DNA sequencing data. *Genome Res.* **20**, 1297–1303 (2010).
48. A. Abyzov, A. E. Urban, M. Snyder, M. Gerstein, CNVnator: An approach to discover, genotype, and characterize typical and atypical CNVs from family and population genome sequencing. *Genome Res.* **21**, 974–984 (2011).
49. M. Jelani *et al.*, A mutation in the major autophagy gene, WIPI2, associated with global developmental abnormalities. *Brain* **142**, 1242–1254 (2019).
50. W. C. Skarnes *et al.*, A conditional knockout resource for the genome-wide study of mouse gene function. *Nature* **474**, 337–342 (2011).
51. J. K. White *et al.*; Sanger Institute Mouse Genetics Project, Genome-wide generation and systematic phenotyping of knockout mice reveals new roles for many genes. *Cell* **154**, 452–464 (2013).
52. E. Ryder *et al.*; Sanger Mouse Genetics Project, Rapid conversion of EUCOMM/KOMP-CSD alleles in mouse embryos using a cell-permeable Cre recombinase. *Transgenic Res.* **23**, 177–185 (2014).